JMEPEG (2011) 20:359–367
DOI: 10.1007/s11665-010-9682-5

1059-9495/$19.00

Effects of Welding Processes and Post-Weld Aging Treatment on Fatigue Behavior of AA2219 Aluminium Alloy Joints

S. Malarvizhi and V. Balasubramanian

(Submitted December 30, 2009; in revised form April 23, 2010)

AA2219 aluminium alloy square butt joints without filler metal addition were fabricated using gas tungsten arc welding (GTAW), electron beam welding (EBW), and friction stir welding (FSW) processes. The fabricated joints were post-weld aged at 175 °C for 12 h. The effect of three welding processes and post-weld aging (PWA) treatment on the fatigue properties is reported. Transverse tensile properties of the welded joints were evaluated. Microstructure analysis was also carried out using optical and electron microscopes. It was found that the post-weld aged FSW joints showed superior fatigue performance compared to EBW and GTAW joints. This was mainly due to the formation of very fine, dynamically recrystallized grains and uniform distribution of fine precipitates in the weld region.

Keywords AA2219 aluminium alloy, electron beam welding, fatigue properties, friction stir welding, gas tungsten arc welding, post-weld aging treatment

1. Introduction

AA2219 is basically Al-Cu-Mn ternary alloy with the minor additions of Ti, V, and Zr. It has been the main workhorse material for applications at cryogenic temperatures. It is the most widely and successfully used cryogenic aluminium alloy and flown in various launch vehicles (Ref 1). It has good combination of strength and toughness at cryo temperatures coupled with excellent weldability that has made this alloys an obvious choice for fabrication of cryogenic tanks (Ref 2).

Many of the structural components in pressure vessels, transport vehicles, earthmoving equipment, spacecraft, etc. are made of welded joints. The butt welds are the most common modes in the fabrication and construction of many structures. The wide application of butt welds in various structures, including offshore, nuclear, and spacecraft, gives large scope for the researchers to analyze the behavior under different types of loading conditions (Ref 3). Failure analysis of the weldments indicated that fatigue alone is to be considered to account for most of the disruptive failures (Ref 4). Even though the fatigue properties of the weld metal are good, problems can be caused when there is an abrupt change in section caused by excess weld reinforcement, undercut, slag inclusion, and lack of penetration, nearly 70% of fatigue cracking occurs in the welded joints (Ref 5).

S. Malarvizhi and **V. Balasubramanian**, Centre for Materials Joining & Research (CEMAJOR), Department of Manufacturing Engineering, Annamalai University, Annamalai Nagar (P.O) 608 002, India. Contact e-mail: visvabalu@yahoo.com.

Though AA2219 has got an edge over its counterparts in terms of weldability, it also suffers from poor as welded (AW) joint tensile and fatigue strength. The joint strength is only about 40% when compared to the base metal strength in T87 condition. The gap between strength values of the base metal and weld metal, particularly yield strength values, is significantly large, forcing the design engineers to use thicker base metal plates, which in turn increases the total weight of the structure (Ref 6). This fact is of concern in aerospace applications because, use of thicker plates due to low yield strength of the weld metal results in lowering of the payload (Ref 7).

It has been shown, many times, that normal engineering tests, such as the static tensile test or the Charpy impact test, are of little value in determining fatigue behavior, particularly of fabricated structures. Maddox (Ref 8) opined that the only way to obtain a quantitative measure of fatigue strength is to carry out fatigue tests under controlled conditions. Fatigue resistance data for design are usually expressed in terms of *S-N* curves, relating nominal applied cyclic stress range *S* and the corresponding number of cycles *N* needed to cause failure. The *S-N* curves used in fatigue design depend on the procedure being used, and by far the most common approach is to use *S-N* curves obtained from fatigue tests on specimens containing the weld details of interest. Such *S-N* curves appear in many codes and standards, including some that apply to welded aluminium alloys (Ref 9).

From the literature review, it is understood that most of the published studies (Ref 10-12) have focused on tensile properties and microstructural characterization of welded AA2219 aluminium alloy. Very few research studies have been published so far on the fatigue behavior of welded AA2219 aluminium alloy joints. Hence, in this investigation, an attempt was made to enhance fatigue performance of gas tungsten arc welded (GTAW), electron beam welded (EBW), and friction stir welded (FSW) AA2219 aluminium alloy joints by post weld aging (PWA) treatment. The effect of welding processes and PWA treatment on fatigue behavior of welded AA2219 aluminium alloy joints is detailed in this article.

2. Experimental Work

The rolled plates of AA2219-T87 aluminium alloy were cut and machined to the required sizes (300 mm × 150 mm × 5 mm) by power hacksaw cutting and grinding. The chemical composition of the base metal is given in Table 1. Square butt joint configuration, as shown in, Fig. 1(a), was prepared to fabricate GTAW, EBW, and FSW joints without filler metal additions. GTAW joints were fabricated using Lincoln (USA) welding machine with 400 A capacity. EBW joints were fabricated using an Electron Beam welding machine (Techmeta, France) with 100 kV capacity. FSW joints were fabricated using an indigenously designed and developed FSW machine (15 HP; 3000 rpm; 50 kN) using a nonconsumable high carbon steel tool. Trial experiments were carried out, and specimens cut at various sections of joint were subjected to macrostructural analysis. Being free from volumetric defect and lack of penetration were considered as the optimized conditions for the specimens. The welding conditions and process parameters are presented in Table 2.

Mechanical and metallurgical properties of the joints were evaluated immediately after the fabrication of joints, without giving any heat treatment, to obtain AW joint properties. PWA treatment was carried out at 175 °C for a soaking period of 12 h. Under this condition, AA2219-T87 alloy attains maximum hardness (Ref 13). Joints were placed into the induction furnace and heated from room temperature to the soaking temperature at a rate of 100 °C/h. After completion of the soaking period, the joints were cooled down in the furnace to room temperature.

The welded joints were sliced using power hacksaw and then ground using surface grinding machine to the required dimensions. Unnotched fatigue specimens were prepared, as shown in Fig. 1(b), from welded joints in the transverse direction (normal to the welding direction) to evaluate the fatigue life. Notched fatigue specimens were also prepared, as shown in Fig. 1(c), from welded joints to evaluate the fatigue notch and notch sensitivity factors. The fatigue testing experiment was conducted at five different stress levels. All the experiments were conducted under uniaxial tensile loading

Table 1 Chemical composition (wt.%) of base metal

Type of material	Cu	Mn	Fe	Zr	V	Si	Ti	Zn	Al
Base metal (AA 2219-T87)	6.33	0.34	0.13	0.12	0.07	0.06	0.04	0.02	Bal

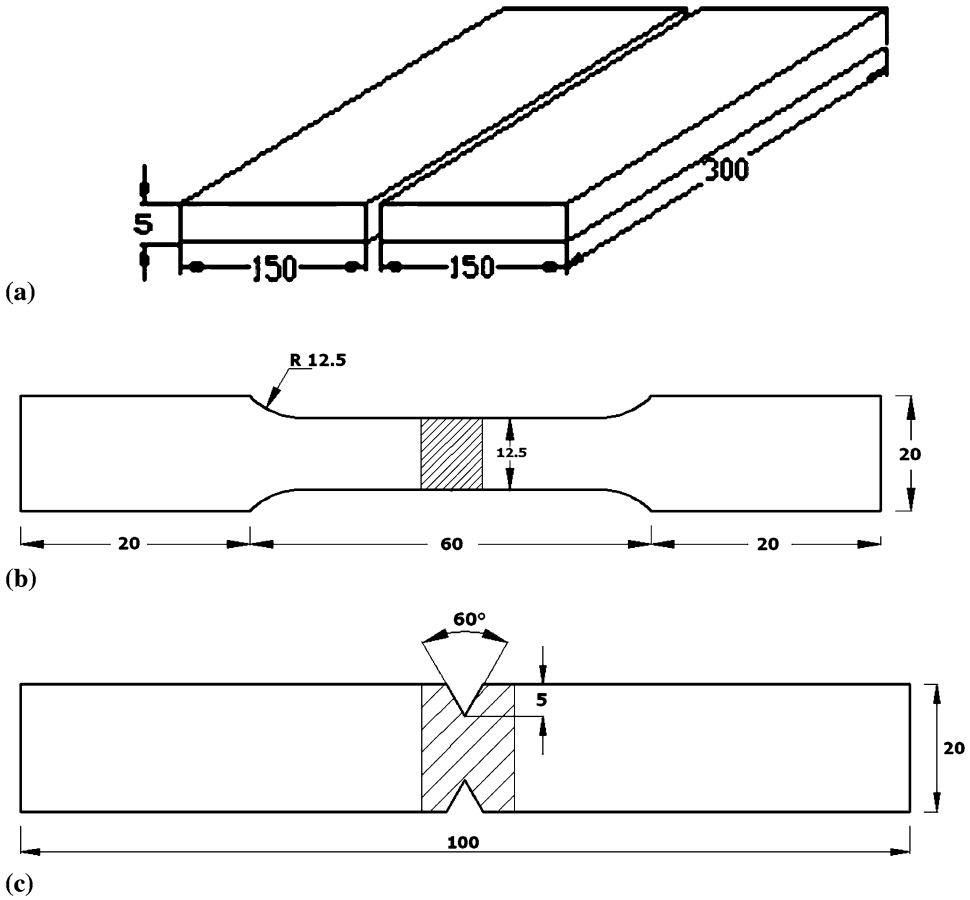

Fig. 1 Configuration of joint and test specimen. (a) Dimension of square butt joint, (b) unnotched fatigue/tensile specimen, (c) notched fatigue specimen

Table 2 Welding conditions and process parameters

Parameter	GTAW	EBW	FSW
Current	150 A	51 mA	
Voltage	30 V	50 kV	
Speed	3 mm/s	16 mm/s	1.5 mm/s
Polarity	AC	DC	…
Vacuum	…	10^{-4} bar	
Shielding gas	99.99% pure argon	…	…
Gas flow rate	10 L/min	…	…
Tool rotational speed			1400 rpm
Axial force			12 kN
FSW tool details			Threaded pin with 6 mm diameter and 4.8 mm length made of high carbon steel

condition (stress ratio = 0) using servo hydraulic fatigue testing machine INSTRON, UK; Model: 8801. At each stress level, three specimens were tested, and the average of the test results are used to plot *S-N* curves.

Transverse tensile specimens were prepared as shown in Fig. 1(b), and American Society for Testing of Materials (ASTM) E8M-04 guidelines were followed for preparing the test specimens. Tensile testing was carried out in 100 kN, electromechanically controlled Universal Testing Machine FIE-BLUE STAR, India Model: 98410. The specimen was loaded at the rate of 1.5 kN/min as per ASTM specifications. The 0.2% offset yield strength was derived from the load-elongation diagram. The percentages of elongation and of reduction in cross-sectional area were evaluated.

Vicker's microhardness testing machine Matzusawa, Japan, Model: MMT-X7 was employed for measuring the hardness of the weld region with 0.05 kg load. Microstructural analysis was carried out using a light optical microscope MEIJI, Japan, Model: ML7100 incorporated with an image analyzing software (Clemex-Vision). The specimens for microstructural analysis were sectioned to the required size from the joint comprising weld metal. They were polished using different grades of emery papers. Final polishing was done using the diamond compound (1 μm particle size) in the disk-polishing machine. Specimens were etched with Kellers reagent to reveal the microstructure. Transmission electron microscope PHILIPS, Model: CM20 was used to get more information about sizes of the precipitates and the distribution of precipitates.

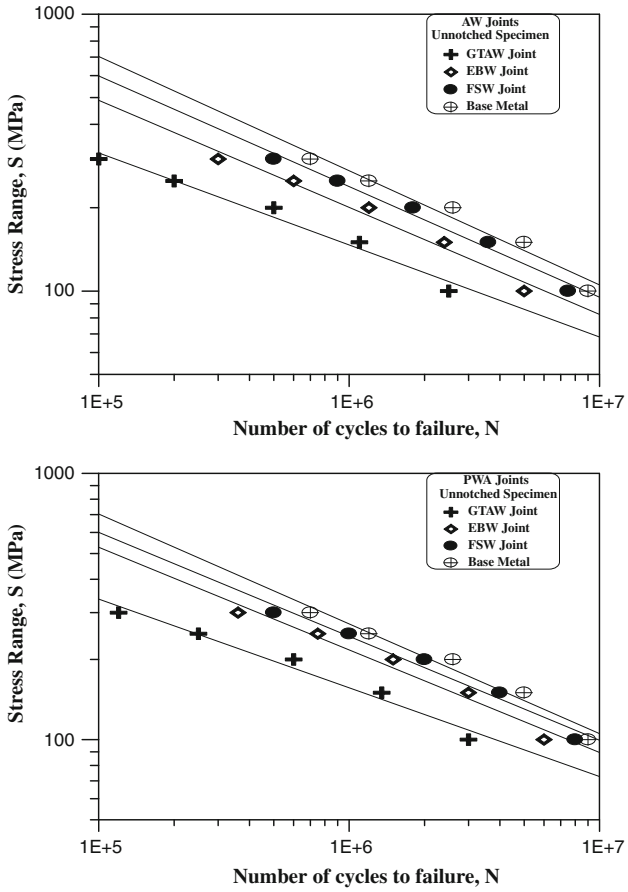

Fig. 2 *S-N* curves of unnotched specimen

3. Results

3.1 Fatigue Properties

Figure 2, shows the fatigue life of AW and post-weld aged unnotched specimens in the form of *S-N* curves. The effect of welding processes and PWA treatment on fatigue life of the joints is revealed by these figures. The *S-N* curve in the high cycle fatigue region is represented by the Basquin equation (Ref 14)

$$S^n N = A \qquad \text{(Eq 1)}$$

where '*S*' is the stress amplitude, '*N*' is the number of cycles to failure and '*n*' and '*A*' are empirical constants. Each *S-N* curve, shown in Fig. 2, can be represented by the above equation. From those equations, the empirical constants '*n*' (slope of the curve) and '*A*' (intercept of the curve) were evaluated, and these are presented in Table 3 and 4.

When comparing the fatigue strengths of different welded joints subjected to similar loading, it is convenient to express fatigue strength in terms of the stresses corresponding to particular lives, for example, 10^5, 10^6, and 10^7 cycles on the mean *S-N* curve. The choice of reference life is quite arbitrary: 2×10^6 cycles has been used, and indeed, some design codes refer to their *S-N* curves in terms of the corresponding stress range (Ref 15). For these reasons, in this investigation, the

Table 3 Fatigue properties of as welded (AW) joints

Joint type	Slope of the *S-N* curve (*n*)	Intercept of the *S-N* curve (*A*)	Fatigue strength of unnotched specimens at 2×10^6 cycles, MPa	Fatigue strength of notch specimens at 2×10^6 cycles, MPa	Fatigue notch factor (K_f)	Notch sensitivity factor (q)
BM: base metal	−0.42	81377	200	110	1.82	0.33
GTAW joints	−0.33	14541	110	50	3.21	0.75
EBW joints	−0.36	41976	150	55	2.73	0.69
FSW joints	−0.39	59689	180	80	2.19	0.48

Table 4 Fatigue properties of post weld aged (PWA) joints

Joint type	Slope of the *S-N* curve (*n*)	Intercept of the *S-N* curve (*A*)	Fatigue strength of unnotched specimens at 2×10^6 cycles, MPa	Fatigue strength of notch specimens at 2×10^6 cycles, MPa	Fatigue notch factor (K_f)	Notch sensitivity factor (*q*)
BM: base metal	−0.42	81377	200	110	1.82	0.33
GTAW joints	−0.35	15656	120	60	2.95	0.61
EBW joints	−0.39	44691	170	70	2.19	0.48
FSW joints	−0.41	73256	190	90	1.90	0.36

fatigue strength of welded joints at 2×10^6 cycles was taken as endurance limit for comparison. The endurance limits were evaluated for all the joints, and they are presented in Table 3 and 4.

The fatigue strength of unwelded AA2219 aluminium alloy is 200 MPa. All the three welding processes are found to be detrimental on fatigue strength of AA2219 aluminium alloy, and it is clearly evident from Fig. 2(a). Of the three AW joints, the joints fabricated by FSW process exhibited very high fatigue strength value. The fatigue strength of FSW joint is 180 MPa which is 10% lower compared to that of the base metal. EBW joint shows fatigue strength of 150 MPa which is 25% lower than that of the base metal. GTAW joint shows the lowest fatigue strength of 110 MPa which is 45% lower than that of the base metal.

Among the three post-weld aged joints, the FSW joint exhibited the highest fatigue strength value. The fatigue strength of post-weld aged FSW joint is 190 MPa and it is 10% higher compared to the fatigue strength of AW FSW joint. The fatigue strength of post-weld aged EBW joint is 170 MPa which is 12% higher than the AW EBW joint. The post-weld aged GTAW joint showed the lowest fatigue strength of 120 MPa which is 10% higher than that of the AW GTAW joint.

Slope of the *S-N* curve is another measure to understand the fatigue performance of welded joints. If the slope of the *S-N* curve is larger, then the fatigue life will be higher and vice versa (Ref 15). The unwelded parent metal showed the highest slope, and the GTAW joint shows the lowest slope under AW and post-weld aged conditions.

The introduction of notch will alter the stress distribution at the vicinity of notch, and the stress value will be magnified near the tip of the notch, which had a definite effect on fatigue life of the components. Hence, in this investigation, fatigue notch and notch sensitivity factors are calculated to evaluate the effect of notches on fatigue life of welded joints. The effect of notches on fatigue strength is determined by comparing the *S-N* curves of notched and unnotched specimens. The data for notched specimens, Fig. 3, are usually plotted in terms of nominal stress based on the net section of the specimen. The effectiveness of the notch in decreasing the fatigue limit is expressed by the

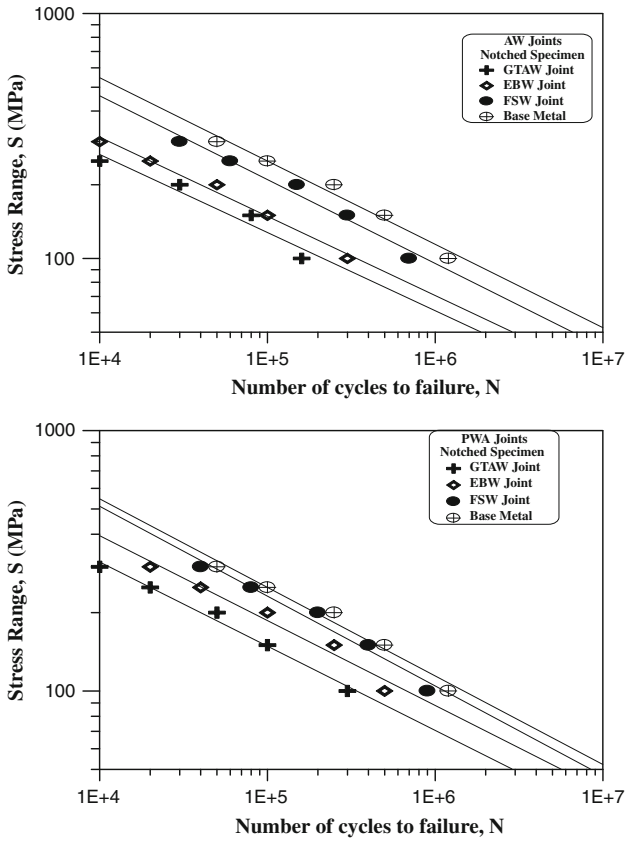

Fig. 3 *S-N* curves of notched specimen

fatigue strength reduction factor or fatigue notch factor, K_f. The fatigue notch factor for all the joints were evaluated using the following expression (Ref 16) and they are given in Table 3 and 4.

$$K_f = \text{Fatigue limit of unnotched specimen/Fatigue limit of notched specimen} \quad \text{(Eq 2)}$$

The notch sensitivity of a material in fatigue is expressed by a notch sensitivity factor 'q' and can be evaluated using the following expression (Ref 16)

$$q = (K_f - 1)/(K_t - 1) \quad \text{(Eq 3)}$$

where K_t is the theoretical stress concentration factor and is the ratio of maximum stress to nominal stress. Using the above expression, fatigue notch sensitivity factor 'q' was evaluated for all the joints, and they are presented in Table 3 and 4.

The fatigue notch factor of unwelded AA2219 aluminium alloy is 1.82. However, the fatigue notch factor of AW joint is 2.73. Among the three AW joints, the FSW joint exhibits very low fatigue notch factor value and the GTAW joint shows very high fatigue notch factor value. Similar trend is observed in notch sensitivity factor values also since it is derived using fatigue notch factor values. The PWA treatment is found to be beneficial to reduce the severity of notches on fatigue life joints, irrespective of welding process. In general, if the fatigue notch factor is lower, then the fatigue life of the joints will be higher and vice versa (Ref 16).

3.2 Tensile Properties

The experimentally evaluated transverse tensile properties of welded AA 2219 aluminium alloy joints are presented in Table 5 and 6, and all the values are the averages of three results. The unwelded parent metal showed a yield strength and tensile strength of 390 and 470 MPa, respectively. Among the three AW joints, the GTAW joints showed the lowest yield strength and tensile strength of 220 and 242 MPa, respectively. This suggests that there is a 50% reduction in strength values due to GTA welding. FSW joints showed the highest yield strength and tensile strength of 305 and 342 MPa, respectively. Though these values are lower than those of the base metal, the strength values are 40% higher than GTAW joints. EBW joints showed the yield strength and tensile strength of 265 and 304 MPa, respectively, which is 30% higher than GTAW joints but 15% lower than FSW joints.

The unwelded parent metal showed an elongation and reduction in cross-sectional area (c.s.a.) of 15 and 10.5%. Among the three welded joints, the GTAW joints showed the lowest elongation and reduction in c.s.a. of 8.8 and 6.2%, respectively. This suggests that there is a 40% reduction in ductility values due to GTA welding. FSW joints showed the highest elongation and reduction in c.s.a. of 12.2 and 8.6%, respectively. Though these values are lower than those of the base metal, the ductility values are 40% higher than GTAW joints. EBW joints also showed an elongation and reduction in c.s.a. of 10.4 and 7.5%, respectively, which is 20% higher than GTAW joints but 15% lower than FSW joints. All the joints showed a 10% enhancement in tensile properties due to the PWA, and this is evident from the results presented in Table 6.

3.3 Hardness

The base metal (unwelded parent metal) in its initial T_{87} condition showed a hardness value of 140 Hv. The hardness is greatly reduced in the weld region, irrespective of welding processes (Table 7). This is one of the reasons for the location of failure invariably at the weld region. GTAW joint showed the lowest hardness of 90 Hv at the weld center. This suggests that the hardness is reduced by 50 Hv in the weld center due to welding heat. FSW joint showed highest hardness of 110 Hv at the weld center. Though this value is much lower than that of the base metal, it is 20 Hv higher than that of GTAW joint, and 5 Hv higher than that of EBW joint. The PWA) treatment increased the hardness of the weld region of all the joints.

Table 7 Microhardness (Hv) of the weld region

Joint type	As welded (AW) joint	Post weld aged joint
BM	140	140
GTAW	90	100
EBW	105	117
FSW	110	124

Table 5 Transverse tensile properties of as welded (AW) joints

Joint type	Yield strength, MPa	Ultimate tensile strength, MPa	Elongation, %	Reduction in cross sectional area, %	Notch tensile strength, MPa	Notch strength ratio (NSR)	Joint efficiency, %
BM	390	470	15.0	10.5	442	0.93	…
GTAW	220	242	8.8	6.2	182	0.75	51
EBW	265	304	10.4	7.5	243	0.80	64
FSW	305	342	12.2	8.6	291	0.85	72

Table 6 Transverse tensile properties of post-weld aged joints

Joint type	Yield strength, MPa	Ultimate tensile strength, MPa	Elongation, %	Reduction in cross sectional area, %	Notch tensile strength, MPa	Notch strength ratio (NSR)	Joint efficiency, %
BM	392	475	15.0	10.0	442	0.93	…
GTAW	237	266	9.6	6.8	213	0.80	56
EBW	300	330	11.8	8.3	280	0.85	70
FSW	344	382	13.2	9.1	343	0.90	80

3.4 Microstructure

Optical micrographs of weld region of the joints are displayed in Fig. 4. The weld region of GTAW joint shows coarse grains normal to the welding direction, Fig. 4(a) and (b). The weld region of EBW joint contains very fine grains relative to GTAW joint, Fig. 4(c) and (d). The weld region of FSP joint contains finer grains, Fig. 4(e) and (f), compared to GTAW and EBW joints. However, the size and distribution of strengthening precipitates are not seen clearly in the optical micrographs, and hence, the weld region of the welds were analyzed using TEM (Transmission Electron Microscope).

In AW GTAW joint, the precipitates are completely dissolved in the matrix and very few particles are seen, Fig. 5(a). The fusion zone of AW EBW joint experiences a fast cooling rate, and the resulting material would be like that of solutionized material, Fig. 5(b), with very less amount of undissolved precipitates. In AW FSW joint, the particles are fine and uniformly distributed throughout the matrix, Fig. 5(c).

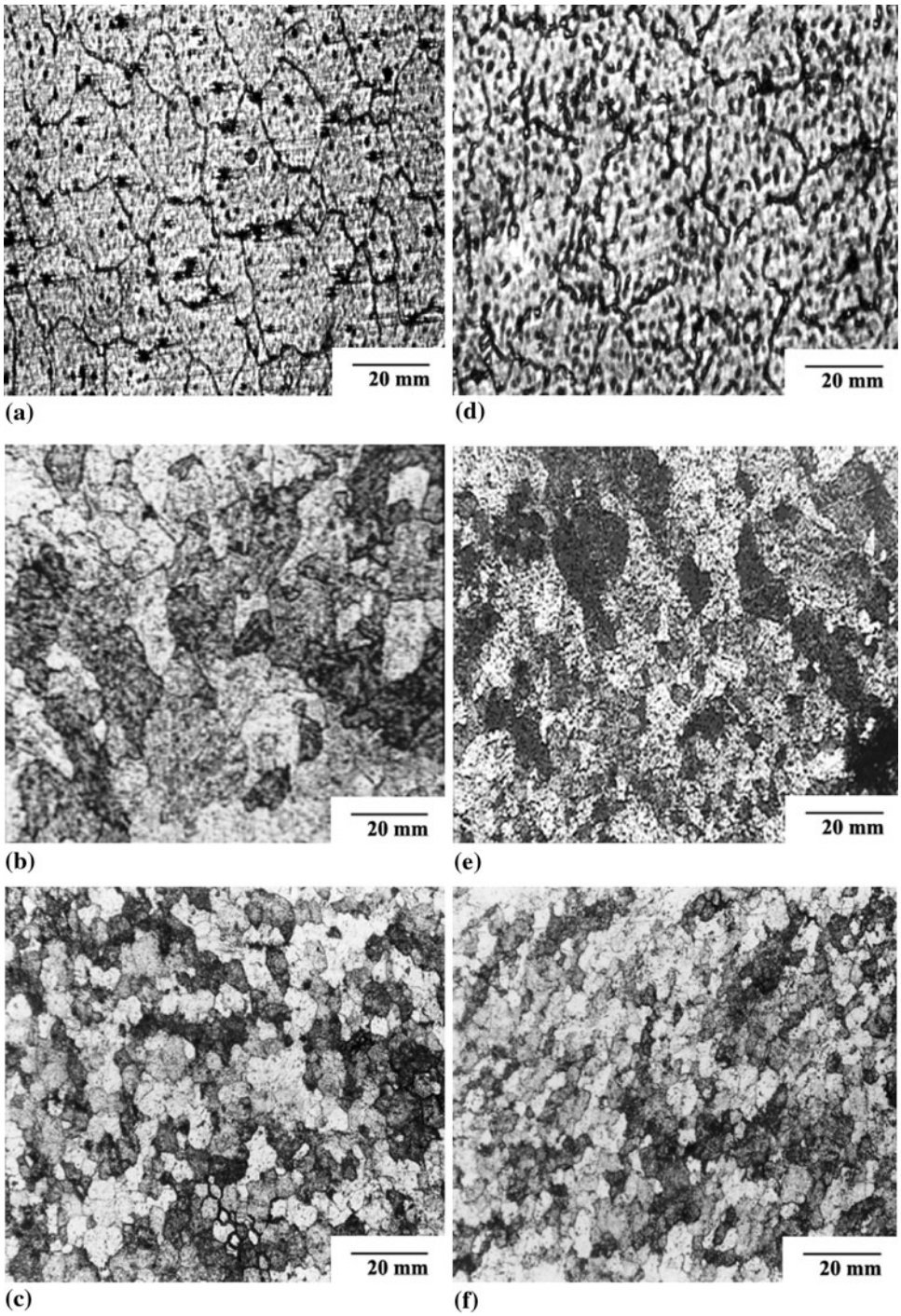

Fig. 4 Optical micrographs of weld region. (a) AW-GTAW, (b) AW-EBW, (c) AW-FSW, (d) PWA-GTAW, (e) PWA-EBW, (f) PWA-FSW

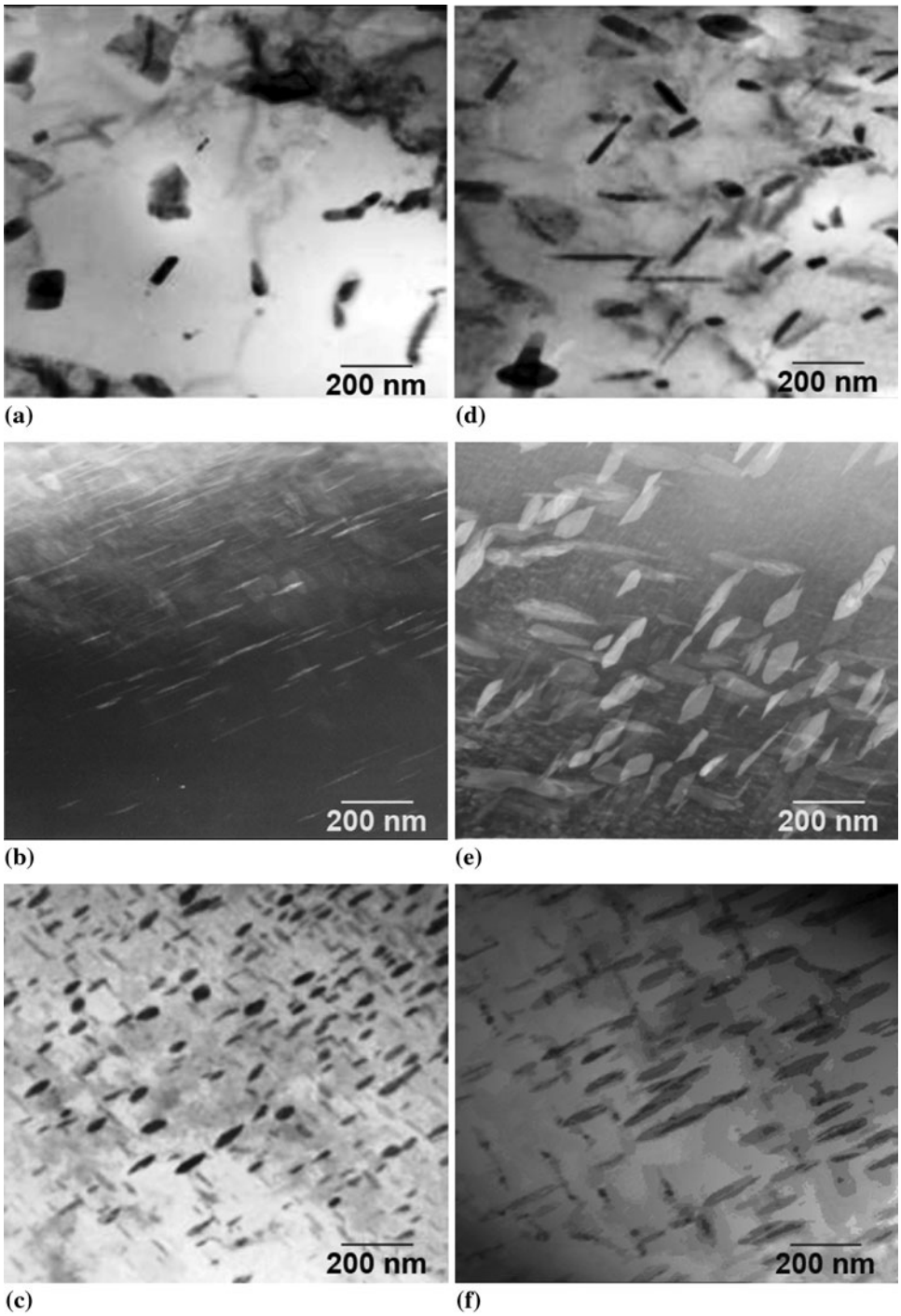

Fig. 5 TEM micrograph of weld region showing precipitates distribution. (a) AW-GTAW, (b) AW-EBW, (c) AW-FSW, (d) PWA-GTAW, (e) PWA-EBW, (f) PWA-FSW

The weld region of post-weld aged joints, Fig. 5(d)-(f), contains more amount of precipitates than that of AW joints, irrespective of welding processes.

4. Discussion

From the above results, it is very clear that the fatigue properties of AA2219 aluminum alloy were greatly reduced by welding processes. Among the six joints, the post-weld aged FSW joint showed better fatigue performance compared to EBW and GTAW joints. The reasons for the better fatigue performance of the post-weld aged FSW joints are (i) superior mechanical properties of the welded joints, (ii) ideal microstructure in the weld region, (iii) preferable size and distribution of strengthening precipitates in the weld region; and (iv) favorable residual stress field in the weld region.

Fine evenly distributed $CuAl_2$ precipitates are the reason for high strength of AA2219 base material. These strengthening

precipitates are formed due to the solution treatment and subsequent artificial aging. During GTA welding, these precipitates are assumed to dissolve, and the weld metal should be left devoid of any precipitates, Fig. 5(a). However, due to the high cooling rates involved in EB welding, not all of them get dissolved and a few of them survive in needleshaped precipitates throughout the matrix, Fig. 5(b). However, in FSW, there is no melting, and hence, there is no dissolution of precipitates in the matrix. The precipitates are due to stirring action of the rotating tool, Fig. 5(c). The weld region of post-weld aged joints, Fig. 5(d)-(f), contains more amount of precipitates than that of AW joints, irrespective of welding processes.

The mechanical properties (yield strength, tensile strength, and elongation) of post-weld aged FSW joints are superior compared to other joints (see Table 5 and 6). The size and distribution of $CuAl_2$ precipitates play a major role in deciding the tensile properties of the welds of AA2219 alloy (Ref 17). It was found that the weld metal region of post-weld aged FSW joint consists of very fine and uniform distribution of precipitates compared to other joints. This was attributed for the superior tensile and hardness properties of post-weld aged FSW joints.

Higher yield strength and tensile strength of the post-weld aged FSW joint is greatly used to enhance the endurance limit of these joints, and hence, the fatigue crack initiation is delayed. Larger elongation (higher ductility) of the post-weld aged FSW joints also imparts greater resistance to fatigue crack propagation, and hence, fatigue crack growth rate is comparatively slow. The combined effect of higher yield strength and higher ductility of the post-weld aged FSW joint offers enhanced resistance to crack initiation and crack propagation, and hence, the fatigue performance of the these joints is superior compared to other joints. Similarly, the uniformly distributed, very fine particles throughout the matrix (weld region) might have impeded the growing fatigue cracks, and hence, the fatigue crack growth rate has been delayed (Ref 18) and, subsequently, the resistance to the fatigue crack propagation has been enhanced compared to other joints.

In the lower strength weld metal, as in the case of GTAW joint, since the deformation and the yielding are mainly concentrated in the weld metal zone, the extension of the plastic zone is limited within the weld metal. As soon as the plastic zone reaches the fusion line, plasticity continues developing along the interface between the parent material and the weld metal (Ref 17). The triaxial state of stress is high in the weld metal, and the relaxation of this stress is poor. The crack driving force needed for crack extension is small. Therefore, the fracture toughness of the lower strength weld metal is not high. On the other hand, if the strength of the weld metal is more or less equal to the base metal, as in the case of post-weld aged FSW joints, then the plastic zone can easily extend into the parent material because the deformation and yielding occur in both the weld metal and the base metal. The stress relaxation can easily take place in the crack tip region. Thus, a higher crack driving force is needed for crack extension, and the fracture resistance of the higher strength weld metal is greater than the lower strength weld metal (Ref 19). This is also one of the reasons for better fatigue performance of the FSW joint.

The magnitude of residual stress in the weld metal region of AW joints is usually tensile. This tensile residual stress field will be normally relieved, if artificial aging treatment is carried out. Hence, in the post-weld aged joints, the magnitude of tensile residual stress field in the weld region will be much lower than that of the AW joints (Ref 20). The higher magnitude of tensile residual stress, usually, will accelerate the growth of fatigue cracks. However, in the post-weld aged FSW joint, the magnitude of residual stress might be lower than that of AW joint. This may be the one of the reasons for the better fatigue performance of post-weld aged FSW joints compared to other joints.

5. Conclusions

From this investigation, the following important conclusions are derived:

(i) The fatigue strength and fatigue life of the AA2219 aluminum alloy were greatly reduced by welding processes. Among the three as-welded joints, the joints fabricated by FSW process exhibited higher fatigue strength and fatigue life compared to GTAW and EBW joints.

(ii) The fatigue notch and notch sensitivity factors of the AA2219 aluminum alloy were increased by welding processes. Among the three welding processes employed in this investigation, FSW process offered better reduction in fatigue notch and notch sensitivity factors compared to GTAW and EBW processes.

(iii) Post-weld aging treatment (PWA) was found to be beneficial to enhance the fatigue strength of the as-welded (AW) joints, by approximately 10-12%. It is also beneficial to reduce the severity of notches under fatigue loading.

(iv) The superior tensile properties (higher yield strength and elongation), ideal microstructures (very fine, dynamically recrystallized grain size), preferable strengthening precipitates (fine and uniformly distributed) and favorable residual stress field (lower magnitude residual stress field) in the weld region are the reasons for superior fatigue performance of the post-weld aged FSW joints.

Acknowledgments

The authors wish to record their sincere thanks to the Aeronautical Research & Development Board (ARDB), New Delhi for the financial support to carry out this investigation under R&D project No. DARO/08/1061356/M1. The authors are grateful to Mr. N. Viswanathan, the retired scientist of the Defence Research & Development Laboratory (DRDL), Hyderabad for providing the EBW facility to carry out this investigation.

References

1. J.A. Hartman, R.J. Beil, and G.T. Hahn, Effect of Copper Rich Regions on Tensile Properties of VPPA Weldments of 2219-T87 Aluminum, *Weld. J.*, 1987, p 73s–83s
2. R.K. Gupta and S.V.S. Narayan, Murty Analysis of Crack in Aluminium Alloy AA2219 Weldment, *Eng. Fail. Anal.*, 2006, **13**(8), p 1370–1375
3. V.V. Yakubovski and I.I. Valteris, Geometrical Parameters of Butt and Fillet Welds and Their Influence on the Welded Joint Fatigue Life, *IIW Doc. No. XIII*, 1989, p 1326–1369
4. C.L. Tsai, Fitness for Service Design of Fillet Welded Joints, *ASCE J. Struct. Div.*, 1986, **112**, p 1761–1780

5. C. Miki and M. Sukano, A Survey of Fatigue Cracking Experience Steel Bridges, *Int. Inst. Weld IIW Doc XIII,* 1990, p 1383–1390
6. G.I. Dance, Comparative Evaluation of Mechanical Properties of TIG, MIG, EBW and VPPA Welded AA2219 Aluminum Alloy, *Weld. Metal Fabric.*, 1994, **24**, p 216–222
7. S.R. Koteswara Rao, G. Madhusudhan Reddy, and K. Prasad Rao, Effects of Thermo-Mechanical Treatments on Mechanical Properties of AA2219 Gas Tungsten Arc Welds, *J. Mater. Process. Technol.*, 2008, **202**, p 283–289
8. S.J. Maddox, Review of Fatigue Assessment Procedures for Welded Aluminium Structures, *Int. J. Fatigue*, 2003, **25**, p 1359–1378
9. A. Hobbacher, Recommendations for Assessment of Weld Imperfections in Respect to Fatigue, *IIW Doc XIII,* 1988, p 1266–1288
10. S. Tosto, F. Nenci, and J. Hu, Microstructure and Properties of Electron Beam Welded and Post Welded 2219 Aluminium Alloy, *Mater. Sci. Technol.*, 1996, **12**, p 323–328
11. A. Kostrivas and J.C. Lippold, A Method of Studying Weld Fusion Boundary Microstructure Evolution in Aluminium alloys, *Weld. J.*, 2000, p 1s–8s
12. S.R. Koteswara Rao, G. Madhusudhana Reddy, K. Srinivasa rao, M. Kamaraj, and K. Prasad Rao, Reasons for Superior Mechanical and Corrosion Properties of 2219 Aluminum Alloy Electron Beam Welds, *Mater. Charact.*, 2005, **40**, p 236–248
13. P. Naga Raju, K. Srinivasa Rao, G.M. Reddy, M. Kamaraj, and K. Prasad Rao, Microstructure and High Temperature Stability of Age Hardenable AA2219 Aluminium Alloy Modified by Sc, Mg and Zr Additions, *Mater. Sci. Eng. A*, 2007, **464**, p 192–201
14. G.E. Dieter, *Mechanical Metallurgy*, 3rd ed., Tata McGraw Hill, New York, 1988
15. R. Jaccard, Fatigue Crack Propagation in Aluminium, *IIW Doc XIII,* 1990, p 1377–1390
16. C.M. Sonsino, Fatigue Assessment of Welded Joints in Al-Mg-4.5 Mn Aluminium Alloy AA 5083 by Local Approaches, *Int. J. Fatigue*, 1999, **21**, p 985–999
17. C. Eripret and P. Hornet, Prediction of Overmatching Effects on the Fracture of Stainless Steel Cracked Welds, *Mis—Matching of Welds*, ESIS 17, K.H. Schwalbe and M. Kocak, Ed., Mechanical Engineering Publications, London, 1994, p 685–708
18. C. Huang and S.Kou, Liquation Cracking in Full Penetration Al-Cu Welds, *Weld. J.*, 2004, p 50s–58s
19. N.B. Potluri, P.K. Ghosh, P.C. Gupta, and Y.S. Reddy, Studies on Weld Metal Characteristics and Their Influences on Tensile and Fatigue Properties of Pulsed Current GMA Welded Al-Zn-Mg Alloy, *Weld. Res. Suppl.*, 1996, p 62s–70s
20. T. Ma, Softening Behaviour of Al-Zn-Mg Alloys Due to Welding, *Mater. Sci. Eng. A*, 1999, **266**, p 198–204